Volume 19, Number 2, 2026. pp. 187-199

Jordan Journal of Physics

ARTICLE

Plasma Characterization in Planar Magnetron Sputtering Systems Using Optical Emission Spectroscopy and Langmuir Probe Diagnostics

Murad M. Kadhim and **Qusay A. Abbas**

Department of Physics, College of Science, Baghdad University, Baghdad, Iraq.

DOI: **https://doi.org/10.47011/19.2.6**

Received on: 10/12/2024; Accepted on: 09/02/2025

Abstract: This study experimentally investigates the fundamental characteristics of glow discharge plasma, including electron temperature, electron density, and plasma potential, which are crucial for optimizing sputtering operations. Optical emission spectroscopy (OES) was utilized to examine spectral lines produced by the plasma, offering a direct assessment of the electron energy distribution. The integration of various diagnostic techniques provides a precise and reliable evaluation of plasma characteristics, enhancing sputtering performance and improving control and efficiency in thin-film deposition. Our findings underscore the synergy between OES and Langmuir probe diagnostics in plasma analysis, while the planar magnetron demonstrates effectiveness in monitoring and optimizing sputtering operations. Furthermore, our findings indicate a significant relationship between gas pressure and the characteristics of glow discharge plasma. Lower pressures facilitate electron transport and increase the plasma potential gradient, whereas higher pressures promote a stable and spatially uniform plasma distribution.

Keywords: Glow discharge, Optical emission spectroscopy, Langmuir probe, I-V curve, Plasma parameters, Beta value.

1. Introduction

Plasma is produced by energizing an inert gas, thereby facilitating energy transfer. High-energy electrons or photons generate electrons and ions when colliding with neutral atoms and molecules in a gas. Plasma generation in a vacuum can be achieved through various methods that supply the requisite energy [1-6]. Magnetron sputtering is a widely used technique in thin-film deposition, providing high-quality coatings for a variety of industrial and scientific applications including semiconductors, optical coatings, and protective layers in industrial applications. Understanding these parameters is important for optimizing the sputtering process and achieving the desired film properties [7-14]. Glow discharge in the sputtering mechanism plays an important role in the plasma discharge process. Key plasma properties that directly affect the total ionization rate, energy distribution among ionized particles, and the deposition rate are electron temperature, electron number density, and plasma potential [15-19]. Two powerful diagnostic techniques for determining plasma properties in dispersion devices are optical emission spectroscopy (OES) and Langmuir probes. OES is a non-destructive approach to observe the emitted light from atoms and ions resulting from plasma excitation. Various plasma parameters like electron temperature and density can be characterized based on the spectral lines. This enables real-time analysis capabilities, which is suitable for dynamic process control. On the other hand, Langmuir probes measure plasma properties by inserting a small probe into the plasma. These probes are capable of measuring electron energy distribution function (EEDF), electron density, and plasma potential [20-22]. Although intrusive, Langmuir probe analysis combined with OES provides highly localized and realistic

Corresponding Author: Murad M. Kadhim **Email**: murad.kadhim1204@sc.uobaghdad.edu.iq

plasma measurements. Application of OES and Langmuir probe analysis provide a comprehensive approach to study the complex behavior of glow discharge plasma in the magnetron sputtering system [23-25].

The novelty of this work lies in the integration of optical emission spectroscopy (OES) and Langmuir probe diagnostics to accurately assess glow discharge plasma properties. This approach optimizes sputtering processes by offering direct measurements of electron temperature, density, and potential. Additionally, the study highlights how varying argon pressure impacts plasma behavior, improving electron transport at lower pressures and stabilizing the plasma at higher pressures, enhancing thin-film deposition efficiency.

2. Theoretical Considerations

2.1 Optical Emission Spectroscopy Method

Electron temperature (T_e), electron density (n_e), Debye length (λ_D), and plasma frequency (ω_{pe}) can all be determined using optical emission spectroscopy (OES). The Boltzmann plot method is particularly effective when the electron excitation temperature (T_e) is considered. This method is widely used in spectroscopic measurements, particularly under the assumption of local thermodynamic equilibrium (LTE), where the Boltzmann distribution is satisfied [26, 27].

$$\ln(\lambda_{ji} I_{ji}/hc\, g_j A_{ji}) = -E_j/k_B T_e + \ln(N/U) \quad (1)$$

where g_j is the statistical weight, h is Planck's constant, k_B is Boltzmann's constant, E_j is the energy of the upper level j, N is the number density of the emitting species, c is the speed of light, and U is the partition function. I_{ji}, λ_{ji}, and A_{ji} represent the intensity, wavelength, and transition probability associated with the transition from level j to level i, respectively. The electron density (n_e) was determined using the Stark broadening effect, which requires a spectral line unaffected by self-absorption [28]:

$$n_e(\mathrm{cm}^{-3}) = \left[\frac{\Delta\lambda}{2\omega_s}\right] N_r \quad (2)$$

where $N_r = 10^{16}$ cm^{-3} is the reference electron density, ω_s is the theoretical line full-width Stark broadening parameter, and $\Delta\lambda$ is the full width at half maximum (FWHM) of the spectral line.

The plasma frequency is expressed as [3]:

$$\omega_{pe} = \sqrt{\frac{n_e\, e^2}{m_e\, \varepsilon_0}} \quad (3)$$

where ε_0 denotes the permittivity of free space, m_e is the electron mass, and e is the electron charge. The Debye length can be determined using the following expression [3]:

$$\lambda_D = \sqrt{\frac{\varepsilon_0\, k_B\, T_e}{e^2\, n_e}} \cong 69\sqrt{\frac{T_e\,(^\circ\mathrm{K})}{n_e\,(\mathrm{m}^{-3})}} \cong 743\sqrt{\frac{T_e\,(\mathrm{eV})}{n_e\,(\mathrm{cm}^{-3})}} \quad (4)$$

2.2 Langmuir Probe Method

The I-V characteristics of a probe describe the relationship between the current (I) flowing through the probe and the applied voltage (V), as shown in Fig. 1. The electron retardation region is characterized by a gradual increase in current with increased voltage. For a Maxwellian distribution, the electron current is given by [29]:

$$I_e = I_{es} \exp\left[\frac{e(V_B - V_p)}{k_B T_e}\right] \quad (5)$$

Taking the natural logarithm of Eq. (5) yields:

$$\frac{d\ln I_e}{dV} = \frac{e}{k_B T_e} \quad (6)$$

Equation (6) demonstrates that the slope of the $(\ln I_e - V)$ is equal to $1/T_e(\mathrm{eV})$, which provides an accurate estimate of the electron temperature. Where: I_e, I_{es}, e, V_B, V_p, k_B, and T_e, represent the electron current, electron saturation current, electron charge, bias voltage, plasma potential, Boltzmann constant, and electron temperature, respectively.

Consequently, the electron density (n_e) can be calculated as follows [29]:

$$n_e = \frac{4 I_{es}}{e\, A_p}\sqrt{\frac{\pi m_e}{8 k_B T_e}} \quad (7)$$

where e, n_e, A_p, k_B, T_e , and m_e denote the electron charge, electron density, probe surface area, Boltzmann constant, electron temperature, and electron mass, respectively.

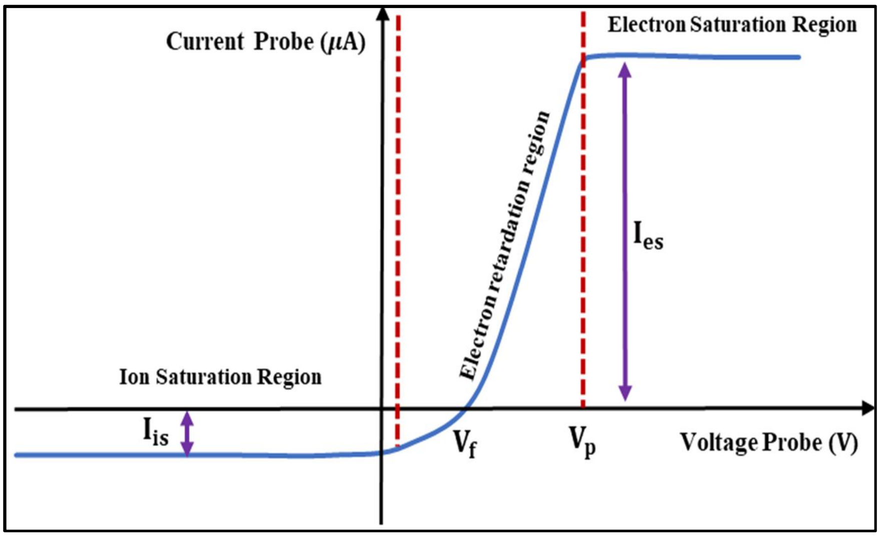

FIG. 1. Typical current-voltage characteristics of Langmuir probe in plasma.

2.3 The concept of β

Analytical evaluation is also performed on the plasma parameter β, which measures the ratio of heat pressure (kinetic energy) to magnetic field pressure (magnetic energy) [30]:

β = Particle or heat pressure/ Magnetic field pressure

$$\beta = \frac{n_e k_B T_e}{(\mathbf{B}^2/2\mu_0)} \tag{8}$$

where $\mathbf{B}^2/2\mu_0$ is the magnetic field pressure. High plasma density generally increases plasma pressure relative to magnetic pressure. The diamagnetic current reduces the magnetic field strength within the plasma. The magnitude of the diamagnetic effect is represented by the ratio of the two terms in Eq. (6). A high plasma beta ($\beta \geq 1$) indicates that plasma pressure becomes comparable to or exceeds the external magnetic pressure thereby reducing the effectiveness of magnetic confinement and allowing greater plasma expansion. In particular, when $\beta > 1$, the plasma pressure exceeds the external magnetic pressure, resulting in weak or unstable confinement. Conversely, when $\beta < 1$, the plasma dynamics are primarily governed by the magnetic field, as observed in magnetic confinement systems where strong magnetic fields are required for plasma confinement [31].

3. Experimental Part

A diagram of the system is presented in Fig. 2. A cylindrical segment of Pyrex glass, 37 cm in length and 30 cm in diameter, was utilized to fabricate the vacuum chamber. The pumping system was connected to one of the two small pipes located at the mid-top and bottom of the chamber, while the other line was employed to inject Argon gas. The two planar electrodes were made of aluminum, each with an inner diameter of 6 cm and an inner length of 3 cm. They were equipped with Teflon to prevent contact with the chamber walls, preserving a 10 cm separation between them. The glow discharge occurring between the electrodes underpins the device's functionality. Applying a continuous DC voltage of around 4 kV across the electrodes induces the formation of an Argon plasma discharge, resulting in a decrease in electrode voltage and the emergence of a characteristic glow discharge. The emission intensity of discharge regions was analyzed using ImageJ software, which enabled precise quantification of pixel intensity variations across the plasma region. The analysis process began with image acquisition, where high-resolution discharge images were captured under controlled experimental conditions. These images were then imported into ImageJ, and background subtraction was applied to eliminate noise and enhance contrast. A region of interest (ROI) was selected to focus on specific discharge areas, ensuring consistent measurements. The software's intensity profiling tool was utilized to extract grayscale values along defined axes, allowing for the visualization of emission distribution. The German-manufactured Thorlabs Optical Emission Spectrometer analyses spatially integrated plasma light emissions throughout the 320-740 nm wavelength range to determine plasma characteristics. The spectrometer was positioned at a 45-degree angle relative to the plasma column. The NIST database software was employed to calibrate spectral results and ascertain plasma characteristics. Cylindrical probes were also designed to investigate the plasma characteristics along the cathode in a singular probe arrangement. The probes included tungsten wires with a diameter of 0.3 mm, insulated save for a brief exposed tip length of 3 mm, and these were placed into a glass tube with a diameter of 4 mm.

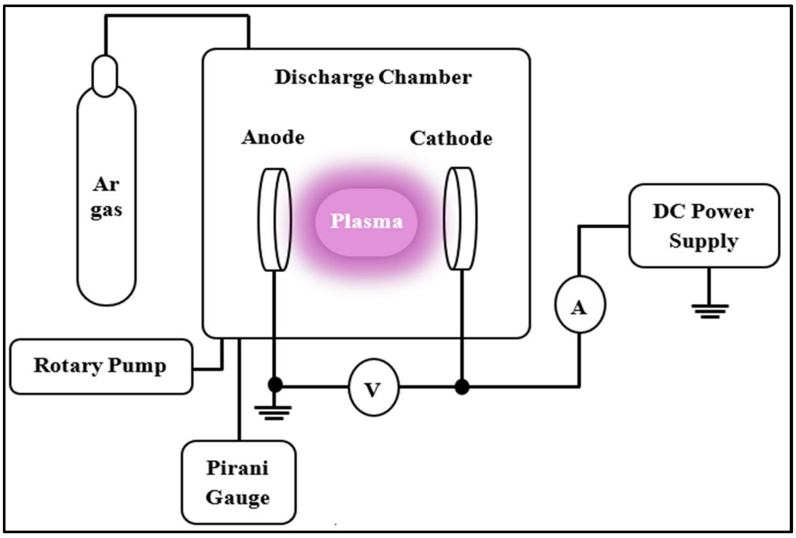

FIG. 2. Schematic of the DC planar magnetron sputtering system.

4. Results and Discussion

4.1 I-V Characteristics

Electrical discharge characteristics in gases are commonly represented by I–V curves, as seen in Fig. 3. In glow-discharge plasma, the current generally increases with applied voltage because higher voltages accelerate electrons to energies sufficient for ionizing gas atoms, thereby increasing the number of charged particles available for conduction. Consequently, the discharge current rises with voltage. However, this relationship is strongly influenced by operating conditions such as gas pressure. The experimental results showed that the I-V curves decreased as the gas pressure increased from 0.04 to 0.4 Torr in the planar magnetron sputtering system. This behavior indicates that gas pressure significantly affects plasma characteristics. At higher pressures, the density of gas particles increases, resulting in more frequent collisions between electrons and gas atoms. Although this can enhance ionization, excessive collisions also reduce electron mobility and mean free path, thereby decreasing the discharge current.

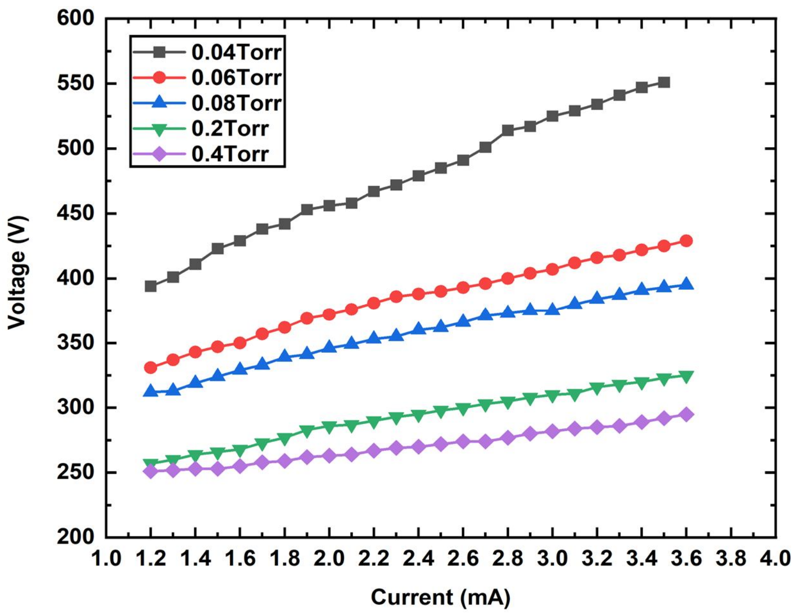

FIG. 3. Effect of variation in working pressure on the current-voltage characteristics.

4.2 Magnetic Field Distribution

Figure 4 depicts the radial distribution of magnetic field dispersion over a flat cathode target. The magnetic field intensified towards the center of the target surface and progressively diminished to a minimum at the cathode edge. This suggests that magnetic confinement was more pronounced in the center portions of the electrode, and the radial magnetic field distribution over the electrode surface is non-uniform.

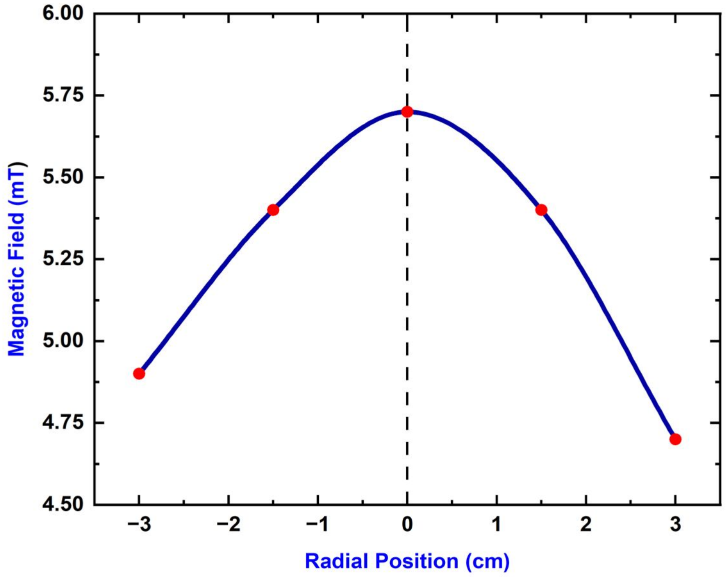

FIG. 4. The magnetic field distribution as a function of radial position (cathode diameter).

4.3 Plasma Emission Intensity

The Image J program is utilized to analyze the areas of discharge emission intensity inside this system. An increase in gas pressure correlates with a rise in the number of discharge zones seen. Fig. 5 illustrates the distribution of light emission intensity throughout the electrode surface (cathode diameter). This figure presents several notable features, including a peak light intensity in the center region of the cathode that gradually decreases toward the cathode edges. Furthermore, the emission intensity was observed to decrease as the gas pressure increased from 0.04 to 0.4 Torr. This behavior is associated with increased gas pressure, which increases the frequency of inelastic collisions between electrons and Ar atoms. Consequently, the reduction in the internal electric field weakens the space-charge effect, thereby reducing the emitted light intensity.

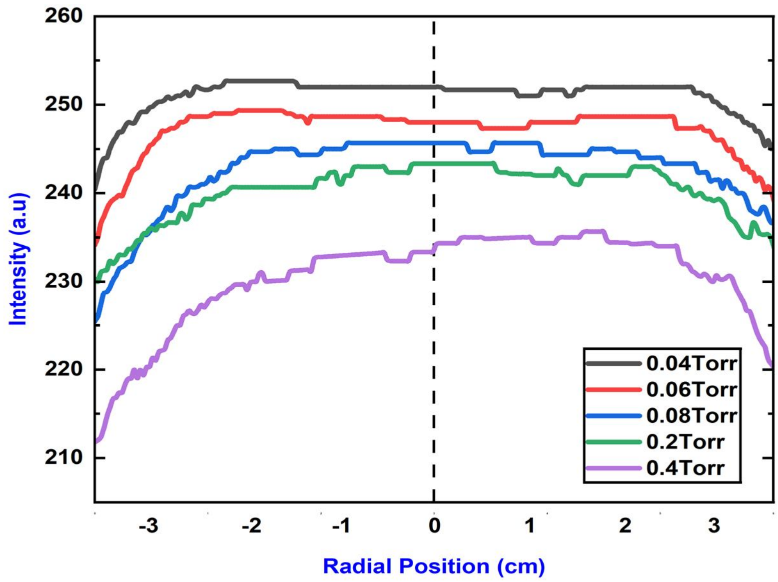

FIG. 5. The variation of plasma emission intensity against radial position.

4.4 Optical Emission Spectroscopy (OES) Method

An optical emission spectrometer detects the emission spectra of argon (Ar) plasma, which is subsequently utilized to analyze the spatially integrated plasma light emissions within the 320–740 nm wavelength range to ascertain plasma parameters. Figure 6 illustrates the Argon (Ar) plasma emission spectrum in a planar magnetron sputtering system at various gas pressures (0.04, 0.06, 0.08, 0.2, and 0.4 Torr). The image delineates many peaks associated with argon neutral atom (ArI) lines, located at wavelengths 549.58730, 591.20850, 603.21270, 617.30960, 656.4224, 675.28340, 696.54300, 706.8730, and 738.39800 nm within the spectrum. Ionic emission lines of ArII were discovered at wavelengths of 337.09150, 357.66150, 380.31720, 391.15760, 419.79458, 427.75280, 434.80640, 460.95670, 476.48640, and 486.13637 nm. The strength of each peak escalates as the gas pressure climbs from 0.04 to 0.4 Torr. This is due to an increase in electron number density, which accelerates the collision rate between electrons and gas atoms, resulting in greater excitation.

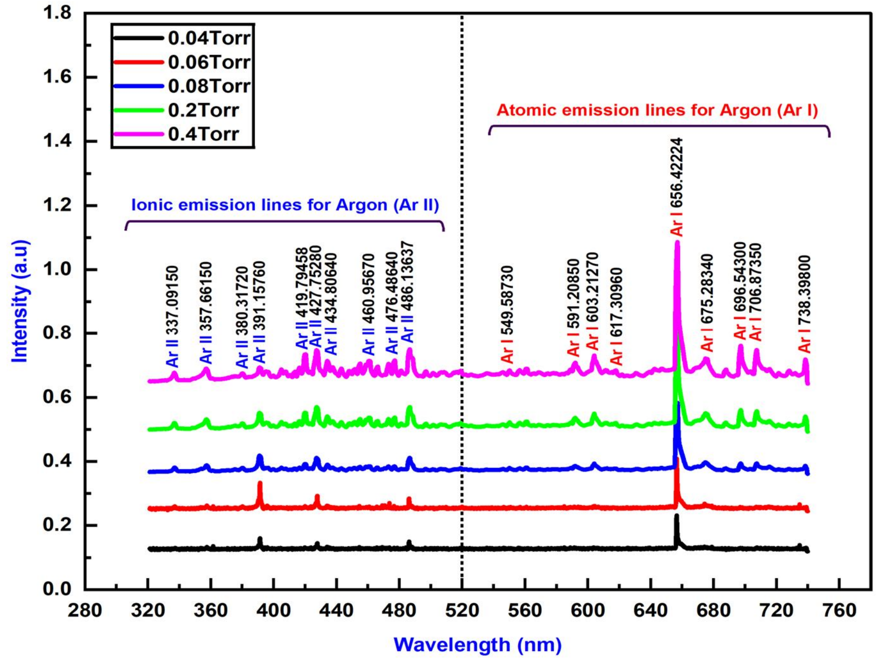

FIG. 6. The optical emission spectra of Argon (Ar) plasma at various gas pressures.

To comprehend the excitation, dissociation, and ionization processes carried out in the plasma, one must be aware of T_e. The slope of the best-fitting line may be used to calculate T_e, which is derived by plotting $\ln(\lambda_{ji} I_{ji}/hc\, g_j A_{ji})$ versus surface energy (E_j). This approach requires data from the NIST database and peaks that come from the same atomic species. Eq. (1), which uses the Boltzmann plot approach, was used to calculate the T_e value using the information given in Table 1. Exploiting the spectral lines released by the atoms and ions in the plasma is one of the most accurate methods for calculating the electron number density (n_e). The Saha-Boltzmann Eq. (2) is used to compute the electron density. The electron number density and the plasma frequency (ω_{pe}) may be computed using Eq. (3). Eq. (4) may be utilized to obtain the Debye length (λ_D), which denotes the shielding distance or the thickness of the plasma sheath. A planar magnetron sputtering system at different gas pressures is shown using the Boltzmann plot method with chosen atomic argon lines (ArI) in Fig. 7.

TABLE 1. ArI standard line characteristics used to determine electron temperature [32].

λ(nm)	$A_{ji} \times g_i$	E_i(eV)	E_j(eV)
549.58730	152×10^5	13.07571571	15.3310400
603.21270	221×10^5	13.07571571	15.13054437
617.30960	34×10^5	13.15314387	15.1610486
656.42224	7.7×10^5	13.07571571	14.97152236
706.87350	60×10^5	13.09487256	14.84836899

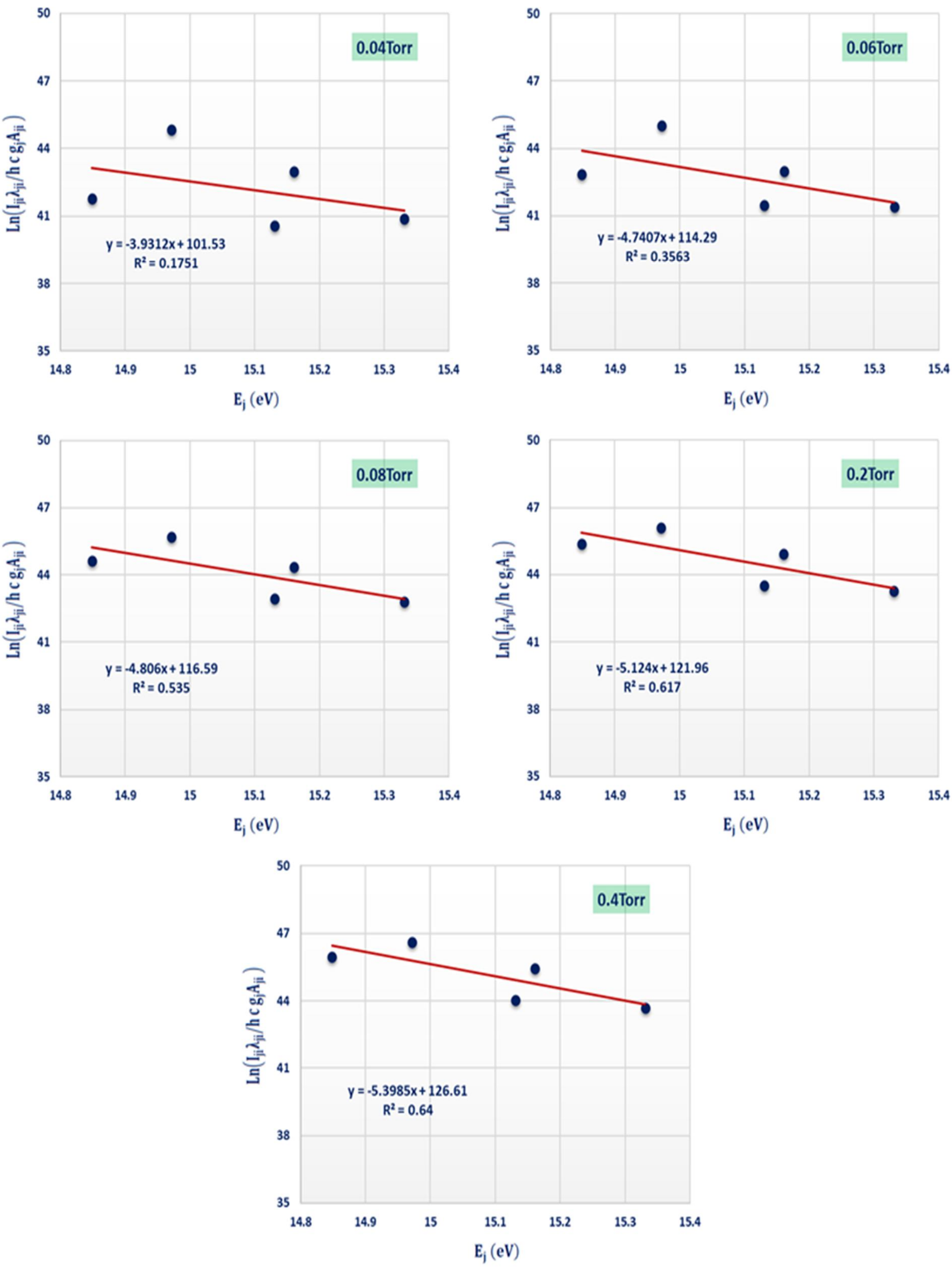

FIG. 7. Boltzmann plot of ArI peaks for a magnetron sputtering system at varying gas pressures.

The relationship between gas pressure and electron temperature (T_e) in a planar magnetron sputtering system is shown in Fig. 8. The data demonstrates a decrease in electron temperature as the gas pressure increases from 0.04 to 0.4 Torr. At lower gas pressures, electrons exhibit longer mean free paths, allowing them to travel greater distances without undergoing frequent collisions with gas atoms. This results in higher electron temperatures, as the electrons retain more energy. As the gas pressure increases, the electrons have a diminished mean free path between collisions with gas atoms, bringing about a lower electron temperature. This loss is due to the energy consumed in such collisions, demonstrating the negative correlation between electron temperature and gas pressure that is important in plasma property control during sputter processes.

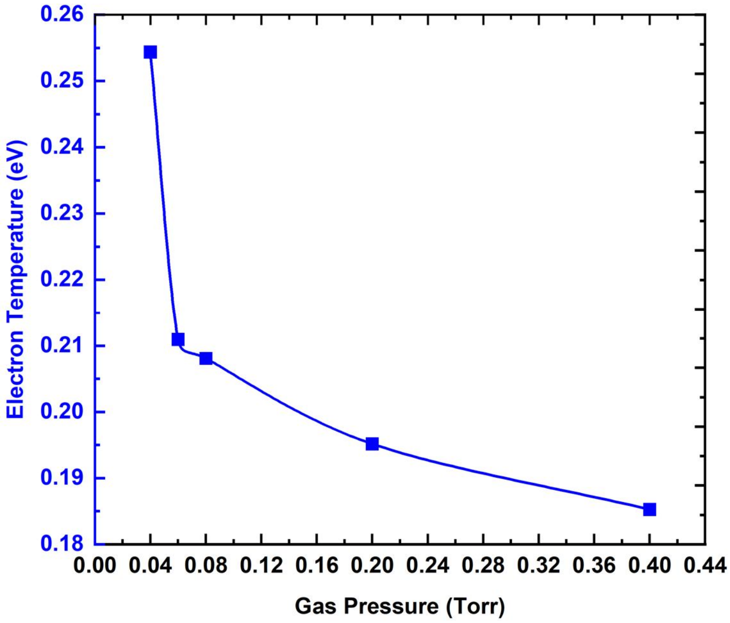

FIG. 8. The variation of T_e with gas pressure in planar magnetron sputtering.

Figure 9 also illustrates the variation of electron density (n_e) with gas pressure in the same planar magnetron sputtering system. The data show that electron density increases as gas pressure rises. Under low gas pressure, the ionization rate is relatively low, resulting in low electron density. However, as gas pressure increases, the frequency of ionization collisions increases due to the high density of neutral gas atoms. This enhanced ionization process increases the number of free electrons, which increases the electron density. The increased collision frequency at elevated pressures therefore improves ionization efficiency, promoting higher electron density that is essential for enhancing the sputtering process and maintaining efficient plasma confinement.

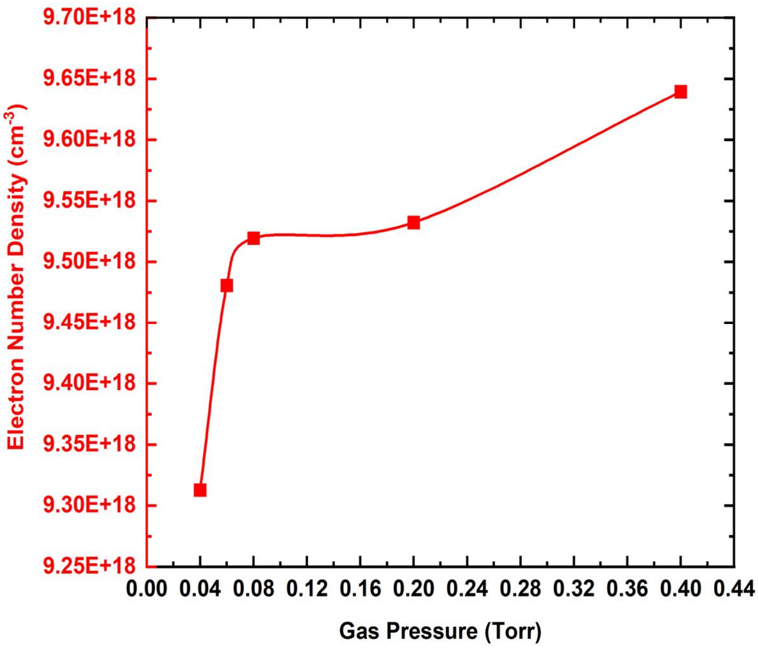

FIG. 9. The variation of n_e with gas pressure in planar magnetron sputtering.

The effect of operating pressure on the Debye length (λ_D) in a magnetron sputtering system is shown in Fig. 10. The results show a clear trend where the Debye length decreases as the gas pressure increases, ranging from 0.04 to 0.4 Torr. A very important parameter of plasma physics, the Debye length characterizes the distance over which electric fields can be screened by the plasma; this depends on both electron temperature and density. With a rise in gas pressure, there is an increase in the number of ionizing collisions, thereby raising the energy of electrons. This increased electron density reduces the Debye length, thereby enhancing the ability of the plasma to screen electric fields over shorter distances. Such a reduction is important for plasma stability and control in sputtering processes because it influences the efficiency of electric field penetration within the plasma.

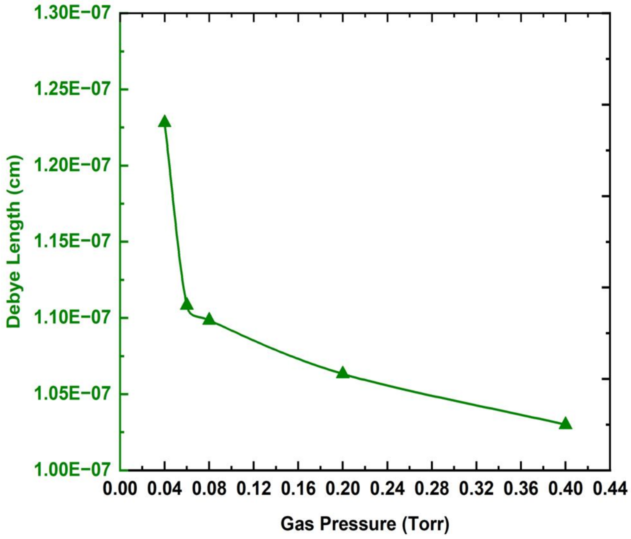

FIG. 10. The variation of λ_D with gas pressure in planar magnetron sputtering.

Figure 11 presents the effect of operating pressure on plasma frequency (ω_{pe}) in the magnetron sputtering system. It follows from this data that the rise of gas pressure automatically involves the growth of plasma frequency. Plasma frequency is determined by electron density and it characterizes the natural frequency of oscillations of electrons in the plasma. As gas pressure increases, more neutral gas atoms and, as a consequence, the probability of ionization collisions increases. These ionization collisions increase the electron density, thereby increasing the plasma frequency. This relationship demonstrates the important role of gas pressure in determining plasma dynamics, since a high plasma frequency indicates an enhanced ability to sustain energetic plasma interactions and thus contributing to high ionization efficiency and overall sputtering performance.

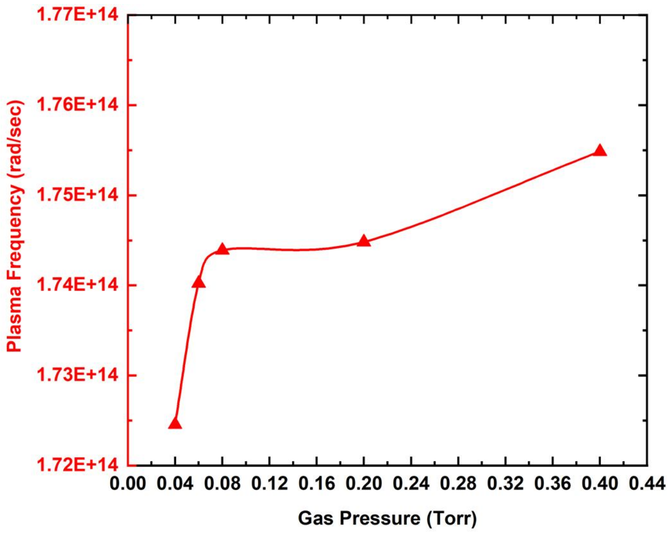

FIG. 11. The variation of ω_{pe} with gas pressure in planar magnetron sputtering.

4.5 Langmuir Probes Method

The slope of the $\ln(I_e) - V$ characteristic curve of the probe was used to calculate the electron temperature, according to Eq. (6). Fig. 12 illustrates the influence of gas pressure on electron temperature behavior at different radial positions. The findings revealed a decrease in electron temperature as gas pressure rose from 0.04 to 0.4 Torr at all radial points (across the cathode diameter). This behavior may be attributed to changes in the gas-discharge characteristics with increasing gas pressure. In particular, inelastic collisions transfer electron energy to gas atoms, thereby reducing electron temperature as gas pressure increases. Consequently, gas temperature rises, while electron temperature and mean electron kinetic energy decrease.

In summary, gas pressure affects electron temperature by altering the collision frequency between electrons and gas molecules. Low-pressure conditions facilitate increased collision-free energy transfer mechanisms, resulting in possible spatial changes in electron temperature. Conversely, collision processes dominate at elevated pressures, resulting in a more uniform electron temperature throughout the gas volume.

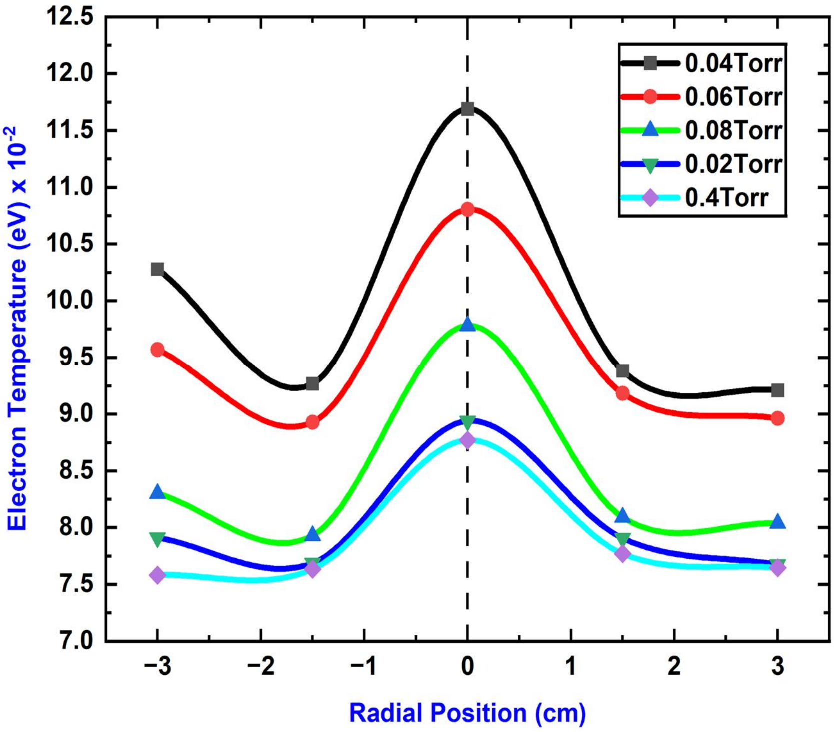

FIG. 12. Variation of electron temperature in plasma with different gas pressures at the cathode diameter (radial position).

An analysis of the relationship between the applied energy and the measured current can provide significant insights into the properties of plasma, including the electron number density. Eq. (7) can be employed to ascertain the stable electron number density. Figure 13 illustrates the impact of gas pressure on electron density at various places. The electron density rate evidently rises with increasing gas pressure at all radial places within the cathode diameter. This may be explained by the fact that an increase in gas pressure results in a greater number of electrons due to enhanced ionization caused by inelastic collisions between electrons and Ar atoms.

In summary, argon pressure influences the plasma density within the sputtering chamber. Elevated pressures often yield denser plasmas, hence augmenting ionisation and enhancing sputtering efficiency. Excessively high pressures may induce plasma instabilities and nonuniform deposition.

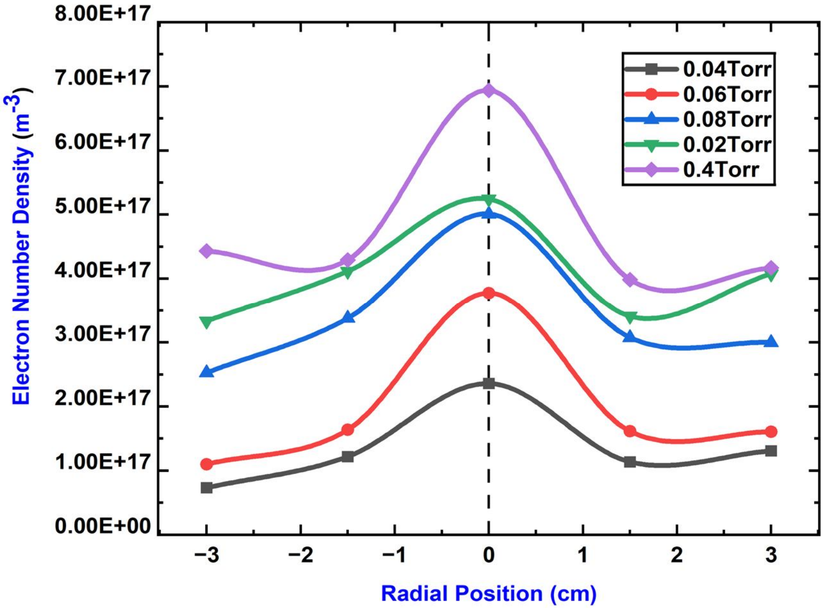

FIG. 13. Variation of electron number density in plasma with different gas pressures at the electrode diameter (radial position).

4.6 Beta Value

The effect of work pressure on the β parameter is determined by Eq. (8) and is calculated in Fig. 14. The results indicate that β exhibits a nonuniform distribution across the electrode surface, with values consistently remaining below 1 at all radial positions. This behavior signifies enhanced plasma confinement, as lower β values are associated with reduced charged particle losses and improved retention of energetic species within the discharge region. This electrode configuration maintains plasma stability by suppressing diffusion and enhancing particle trapping, thereby contributing to sustained ionization processes. Furthermore, the observed variation in β with rising gas pressure is a direct consequence of the enhanced electron number density, which promotes higher ionization rates and reinforces plasma containment. These results demonstrate the importance of operational parameters in governing plasma behavior and emphasize the need to optimize discharge conditions for effective confinement and improved performance in plasma-based applications.

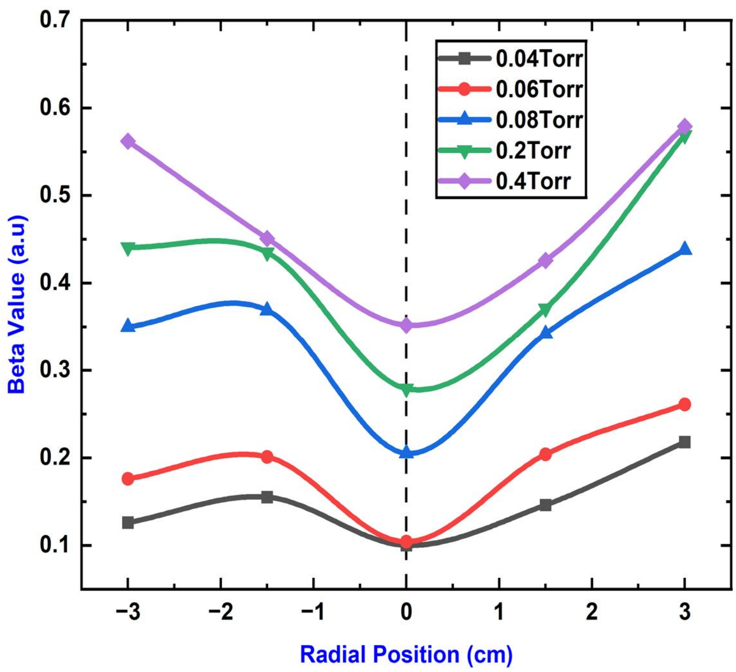

FIG. 14. The variation of β-value as a function of radial position (cathode diameter).

5. Conclusions

In this work, optical emission spectroscopy (OES) was employed to investigate DC discharges in a planar magnetron sputtering system at various gas pressures. The findings showed that electron number density and plasma frequency increased with rising gas pressure, whereas electron temperature and Debye length decreased.

Langmuir probe diagnostics performed at different gas pressures and radial positions revealed that the light intensity peaked in the central region of the cathode and gradually decreased toward the cathode edges. The measurements also confirmed that electron temperature (T_e) decreased while electron number density (n_e) increased as gas pressure increased.

Furthermore, the influence of magnetic field configuration on plasma confinement was evaluated through the plasma beta parameter (β). The measured β values remained below unity throughout the investigated pressure range, indicating effective magnetic confinement despite their gradual increase with gas pressure.

Author Contribution Statement

Murad M. Kadhim and Qusay A. Abbas contributed equally to this work. Murad M. Kadhim was primarily responsible for the conceptualization and design of the study, as well as the development of the methodology and the analysis of the data. Qusay A. Abbas focused on the experimental work, data collection, and initial drafting of the manuscript. Both authors engaged in the review and editing of the manuscript, provided critical revisions, and approved the final version.

Funding

This research received no specific grant from any funding agency in the public, commercial, or not-for-profit sectors.

Data Availability Statement

Some or all data that support the findings of this study are available from the corresponding author upon reasonable request.

Statements and Declarations

This manuscript provides an in-depth analysis of plasma parameter characterization in planar magnetron sputtering, utilizing Optical Emission Spectroscopy and Langmuir probe techniques.

Competing interests

The authors have not disclosed any competing interests.

Acknowledgement

The authors are thankful to the staff at Baghdad University for their cooperation and support.

References

[1] Abdalameer, N.K., Yasoob, N.A., and Mohammed, A.Q., International Journal of Nanoscience, 23 (3) (2024) 2350078-12.

[2] Raizer, Y. P., “Gas Discharge Physics”, (Springer, 1991).

[3] Khalepha, T.A. and Abdalameer, N.K., Baghdad Science Journal, 21 (12) (2024) 35.

[4] Roth, J.R., “Industrial Plasma Engineering”, (CRC Press, 2001).

[5] Khalepha, T.A. and Abdalameer, N.K., Journal of Optics, 53 (2024) 5016.

[6] Khalaf, T.H., Abbas, Q.A., and Kadhim, M.M., Iraqi Journal of Science, 63 (11) (2022) 4771.

[7] Kadhim, M.M., Abbas, Q.A., and Abdulameer, M.R., Iraqi Journal of Science, 63 (5) (2022) 2048.

[8] Matsuda, T. and Endo, T., Thin Solid Films, 442 (1-2) (2003) 1.

[9] Windischmann, H., Critical Reviews in **Solid State** and Materials Sciences, 17 (6) (1992) 547.

[10] Kadhim, M.M. and Abbas, Q.A., Iraqi Journal of Science, 63 (10) (2022) 4254.

[11] Aadim, K.A., Iraqi Journal of Physics, 15 (32) (2017) 57.

[12] Chopra, K.L., “Thin Film Phenomena”, (McGraw-Hill, 1969).

[13] Maniv, S., Journal of Applied Physics, 58 (7) (1985) 2492.

[14] Schiller, S., Heisig, U., and Goedicke, K., J. Journal of Vacuum Science & Technology A: Vacuum, Surfaces, and Films, 1 (2) (1983) 218.

[15] Bogaerts, A. and Neyts, E., ACS Energy Letters, 4 (4) (2019) 922.

[16] Chen, F.F., IEEE Transactions on Plasma Science, 31 (6) (2003) 1257.

[17] Rossnagel, S.M., Journal of Vacuum Science & Technology A: Vacuum, Surfaces, and Films, 6 (1) (1988) 19.

[18] Abbas, Q.A. and Ahmead, R.T., Iraqi Journal of Physics, 13 (26) (2015) 64.

[19] Bard, A.K. and Abbas, Q.A., Iraqi Journal of Science, 63 (8) (2022) 3412.

[20] Algaffar, A.N.A., Abdalameer, N.K., and Tariq, S.Z., International Journal of Nanoscience, 21 (06) (2022) 2250049.

[21] Hutchinson, I.H., "Principles of Plasma Diagnostics", (Cambridge University Press, 2002).

[22] Godyak, V.A. and Piejak, R.B., Physical Review Letters, 65 (8) (1990) 996.

[23] Muraoka, K. and Maeda, T., Journal of Physics D: Applied Physics, 41 (19) (2008) 194008.

[24] Yasoob, N., Abdalameer, N.K., and Mohammed, A.Q., International Journal of Nanoscience, 21 (06) (2022) 2230003.

[25] Bohm, C. and Perrin, J., Review of Scientific Instruments, 64 (1) (1993) 31.

[26] Fantz, U., Plasma Sources Science and Technology, 15 (4) (2006) S137.

[27] Shafeq, O.S., Al-Oubidy, E.A., Mahdi, T.S., and Hameed, M.A., Journal of Optics, 2024 (2024) 1.

[28] Gigosos, M.A. and Cardenoso, V., Journal of Physics B: Atomic, Molecular and Optical Physics, 29 (20) (1996) 4795.

[29] Kadhim, M.M. and Abbas, Q.A., Iraqi Journal of Applied Physics, 20 (3) (2024) 696.

[30] Boyd, T.J.M. and Sanderson, J.J., "The Physics of Plasmas", (Cambridge University Press, 2003).

[31] Raju, M.S., Singh, R.K., Gopinath, P., and Kumar, A., Journal of Applied Physics, 116 (15) (2014) 1.

[32] National Institute of Standards and Technology (NIST), Retrieved from: https://www.nist.gov/pml/atomic-spectra-database (2024).